Unstable periodic orbits in the parametrically excited pendulum

Willem van de Water and Marc Hoppenbrouwers
Physics Department, Eindhoven University of Technology, P.O. Box 513, 5600 MB Eindhoven, The Netherlands

Freddy Christiansen
The Niels Bohr Institute, Blegdamsvej 17, DK-2100 Copenhagen, Denmark
(Received 23 July 1990; revised manuscript received 19 April 1991)

We analyze chaotic motion in an experiment on a parametrically excited pendulum in terms of unstable periodic orbits. This provides a useful quantitative comparison with results of a faithful numerical simulation. Despite the presence of experimental artifacts, simulation and experiment are in good agreement. The analysis of scaling properties of both chaotic attractors along these lines remains, however, incomplete. Periodic-orbit analysis fails to account for their marginal hyperbolicity, and therefore fails to capture an important qualitative aspect of the chaotic dynamics in both experiment and simulation.

PACS number(s): 05.45.+b, 46.10.+z

I. INTRODUCTION

One of the most impressive discoveries in the physics of nonlinear dynamical systems is the universality of their chaotic behavior. For example, a phase-space orbit in a dissipative system may cover a strange attractor whose structure possesses universal features. The scaling properties of this structure can be quantified using scaling functions, such as the spectrum of generalized dimensions D^q. Widely different systems may then be described by identical functions D^q.

It is now recognized, however, that this universality only applies to systems located on the borderline of chaos. Universality shows when special points on this border are approached hierarchically in parameter space. It is expected that universal scaling behavior can no longer be found at the other side of the border. A consequence would then be that one expects an experiment to show different scaling behavior than its theory or numerical simulation.

It is very hard to fabricate a mechanical realization of a differential equation without introducing experimental artifacts. Because nonlinear dynamical systems often exhibit sensitive dependence on parameter settings, these artifacts may essentially alter the dynamics in mind. Since at the other side of the chaos border there no more exists a hierarchical approach that governs navigation through parameter space, the only recourse in the experiment is the theoretical parameter settings. The state of the experimental system may then be essentially different from that found from the differential equation. One might argue that this problem might be posed entirely in the context of numerical simulations where a simulation of a differential equation is compared to one that is made to include more and more "experimental" artifacts. Performing real experiments, however, provides crucial guidance as to which artifacts might be of practical relevance.

Just beyond the chaos border, metric universality, that is, universal scaling behavior of the attractor, may give way to topological universality, i.e., that the attractor has its parts in the proper place. This was quite convincingly demonstrated experimentally by Gunaratne, Linsay, and Vinson [1], who studied an electronic realization of the circle map just beyond criticality where chaotic orbits start to wander out of one-dimensional phase space.

If it is indeed problematic to construct experiments involving chaotic dynamics that has predictable scaling behavior, the question quite naturally arises as to what manner the found differences should be quantified. According to a recent suggestion [2], low-dimensional chaos can be described through its underlying skeleton of unstable periodic orbits. It was Poincaré's original idea that a chaotic dynamical system will after a given time return arbitrarily close to its starting location in phase space [3]. By slightly adjusting the phase-space point, this return can be made exact, and the point is turned into a periodic point. In a low-dimensional chaotic experiment, a registered time series will contain many points that are near a cyclic point and that almost return. These points can be used to estimate the precise location of the cycle, whereas the evolution of their neighborhoods allows an estimate of the stable and unstable cycle eigenvalues. In simple systems the skeleton of periodic points can often be constructed *hierarchically,* and then provides a *complete* description of chaos.

Such a description would be eminently suited to quantify differences between chaotic dynamics as observed in an experiment and as observed in theory or in numerical simulations. In the past few years, several ways have been explored to measure the scaling function D^q in an experiment [4–6]. A periodic-orbit analysis would also furnish this scaling function. At the same time, however, it would give insight into the dynamical mechanism that brings forth the scaling of the experimental measure and it would elucidate the nature of differences between experiment and simulation.

A circumstance that at first sight discourages application of periodic-orbit analysis is the necessity of finding arbitrarily long periods together with their stable and un-

stable eigenvalues. With a finite number of data points measured with finite precision, this is an impossible task. However, it has been shown that in many cases long cycles are shadowed by sequences of nearby short cycles [7]. This circumstance gives rise to cycle expansions: an elegant and systematic manner of approximating the contribution of long cycles by nearby short ones. Thus, by locating only the short cycles in an experiment, one should be able to characterize the dynamics at much longer times. The error made by omitting the true long cycles is expected to diminish rapidly with the increasing length of the included orbits. The rate of convergence, the success of the cycle expansion, is intimately tied to the underlying symbolic dynamics. It is exponential in the case of "well behaved" symbolic dynamics that is, for example, found for one-dimensional (1D) repellers [2,7]. Therefore, in order to assess the performance of a cycle expansion, it is necessary to have a good idea of the symbolic dynamics at hand. This, incidentally, is a nontrivial task when the experiment is not truly low dimensional (i.e., close to one dimensional).

In this paper we analyze chaotic dynamics in a mechanical realization of a parametrically excited damped pendulum: a pendulum whose support is lifted periodically. Ideally, this experiment would be described by the well-known differential equation [8]

$$\frac{d^2\varphi}{dt^2}+\frac{k_2}{ml^2}\frac{d\varphi}{dt}+\left[\omega_0^2-\frac{A\omega^2}{l}\cos(\omega t)\right]\sin\varphi=0\ , \quad (1)$$

where l is the length of the pendulum, m its mass, and where ω_0 is the eigenfrequency for small excursions φ. The pendulum is excited with amplitude A and damped by ordinary friction that is gauged by a damping constant k_2. A few years ago Koch *et al.* [9] constructed a similar mechanical device and uncovered a plethora of nonlinear phenomena, such as period-doubling series and transient chaos. We have improved the accuracy of the experiment and will concentrate on the measurement of scaling properties instead. The principal aim of the present paper is the comparison of a direct method of extracting scaling behavior with the result of a periodic-orbit analysis, both for the experiment as well as for its faithful numerical simulation. We anticipate that a better understanding of these methods, and of their practical implementation in particular, will lead to better tools for analyzing chaos.

In Sec. II of this paper we will analyze the experiment and introduce the differential equation that is assumed to describe it and its numerical simulation. In Sec. III we discuss the measurement of scalings and compare the spectrum of generalized dimensions D^q from the experimental attractor with that of its numerical simulation. The power and elegance of a periodic-orbit analysis have been illustrated in the case of simple dynamical systems consisting of one- or two-dimensional mappings [7]. So far, the full potential of the method to analyze experimental results has remained unexplored [1,10]. In Sec. IV we focus on practical aspects of the implementation of a periodic-orbit analysis of the experiment. We will, therefore, always work with *time series,* even in the case of numerical simulations where, in principle, the periodic orbits and their eigenvalues are directly accessible. It will turn out that a measurement of the stability of the underlying net of unstable cycles points to the dynamical origin of the scaling behavior of the asymptotic measure and is, therefore, often to be preferred over direct methods that merely extract its averaged scaling behavior. However, at the same time we will show that a cycle analysis does not supersede these direct methods.

II. EXPERIMENT

Figure 1 shows the mechanical device. The pendulum is 0.317 m long and terminates in a bob of 0.0858 kg. The support of the pendulum is driven by a crank mechanism. This allows for a more stable and simple construction, although the obvious drawback is that the excitation is no longer described by the second term between the large parentheses in Eq. (1) and contains higher harmonics. The pendulum is driven by a 1-kW motor with a tachogenerator feedback mechanism that keeps the angular velocity ω constant to approximately 4%. An optical encoder with an angular resolution of $2\pi/4096$ gives information about the instantaneous angular position φ of the pendulum. It is interfaced by a logical circuit to a computer that reads φ each time the support is in its highest position. A second reading, 15.08 ms later, is used to obtain the angular velocity coordinate $\dot{\varphi}$ of the point $(\varphi,\dot{\varphi})$ in the Poincaré section; phase-space points

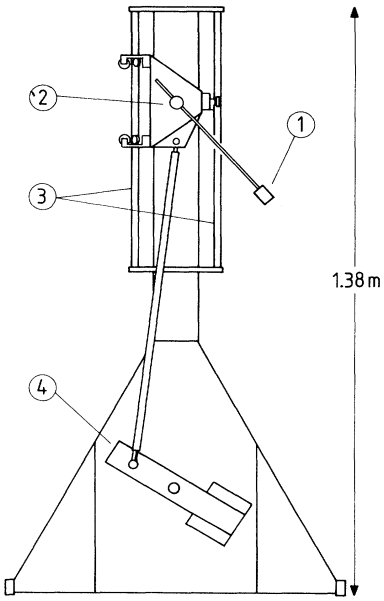

FIG. 1. The parametrically driven pendulum drawn to scale; its height is 1.38 m. 1, bob of 0.0858 kg; 2, suspension with optical angle encoder; 3, rods guiding the vertical motion of the suspension; 4, driving crank.

are thus obtained with time intervals of $2\pi/\omega$. The noise ϵ_n in the $(\varphi,\dot{\varphi})$ measurement was estimated from the accuracy of measured returns in the phase plane when the pendulum was in a sate of periodic motion. Within a few cycles of the excitation, periodic points would be sharp to within 3×10^{-3}, and would broaden to twice this value after about ten cycles.

A faithful simulation of the actual experiment introduces extra terms in Eq. (1) that reflect the presence of other damping forces and that allow for the noticed peculiarity of the excitation. Friction forces other than that represented by the term proportional to $\dot{\varphi}$ will be air resistance that introduces a term proportional to $(\dot{\varphi})^2\mathrm{sgn}(\dot{\varphi})$, whereas the bearings will counteract the motion through a Coulomb friction term that only depends on the sign of $\dot{\varphi}$. Apart from those, there may even be other forces acting in the experiment; for example, small excursions near $\varphi=0$ could be influenced by harmonic forces that are due to imperfections in ball bearings.

In summary, the original equation of motion has to be augmented to

$$\frac{d^2\varphi}{dt^2}+\frac{k_1}{ml^2}\mathrm{sgn}\left[\frac{d\varphi}{dt}\right]+\frac{k_2}{ml^2}\frac{d\varphi}{dt}+\frac{k_3}{ml^2}\left[\frac{d\varphi}{dt}\right]^2\mathrm{sgn}\left[\frac{d\varphi}{dt}\right]+\left[\omega_0^2-\frac{A\omega^2}{l}\left[\cos(\omega t)+\epsilon\frac{\cos(2\omega t)+\epsilon^2\sin^4(\omega t)}{[1-\epsilon^2\sin(\omega t)]^{3/2}}\right]\right]\sin(\varphi)=0\ , \quad (2)$$

where ϵ is the ratio of the two arms that make up the driving crank mechanism. We have measured all three damping parameters k_1, k_2, and k_3 in an unexcited, freely swinging pendulum released at $\varphi=0$ at $t=0$. Figure 2 shows a plot of the excursion maxima as a function of time, together with a prediction based upon Eq. (2) where the damping constants k_1, k_2, and k_3 have been adjusted so as to obtain the best agreement between measurement and simulation [11]. Although we believe that the presence of damping terms that have a more complicated dependence on the angular velocity is unavoidable in any mechanical realization of Eq. (1), their presence will not affect the main conclusions of this paper.

The phase diagram of the parametrically excited pendulum is shown as a function of ω in Fig. 3 where the angular frequency of the excitation is varied from 8 to 13 S^{-1}, which is about the largest angular frequency that is feasible in the experiment. Although there appears to be a shift of the bifurcation values of ω in the experiment, the scenario that gives birth to the chaotic attractor that we wish to study is the same in the experiment and its simulation. At 13 S^{-1} the pendulum is in a rotating motion whose frequency is locked to the excitation. When lowering ω, we encounter a series of period-doubling bifurcations that leads to a small fourfold chaotic attractor at $\omega=9.295$ S^{-1}. At slightly smaller ω this state yields a large chaotic attractor that extends over the full angular range. The noise in the angle measurements obscures further doublings of the period-4 cycle in the experiment. The computed largest period-8 subharmonic amplitude in the simulation ($\Delta\varphi/2\pi=5.0\times10^{-3}$) is consistent with the estimated noise level in the experiment. We notice incidentally that the presence of higher-order harmonic terms in the excitation that have size $\epsilon=0.17$ in Eq. (2) is essential for the sketched scenario.

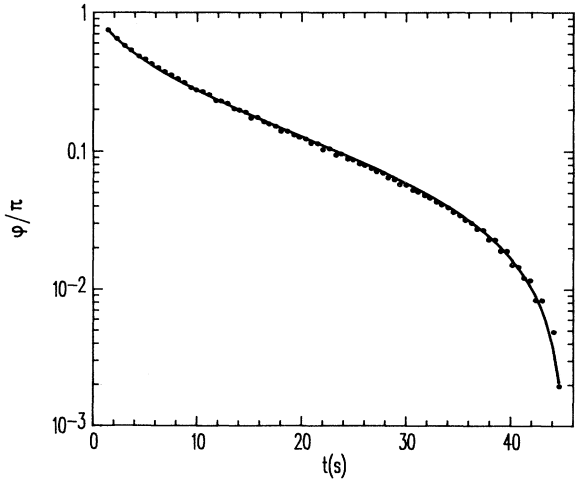

FIG. 2. Excursion maxima ($\dot{\varphi}=0$) of a damped unexcited pendulum as a function of time. Dots, experiment; solid line, a fit using Eq. (2) with $A=0$.

The large chaotic attractor that is shown both for experiment and simulation in Fig. 4 is, in fact, transient. It engulfs the origin that is stable due to the presence of the hysteretic friction term $k_1\mathrm{sgn}(\dot{\varphi})$. The effect of this term is that the pendulum may become still at a finite angle φ [12]. The length of the chaotic transients may be very long. Figure 4 shows a transient that lasted 42 754 cycles. However, since we were interested in much longer simulated time series, we performed all simulations with $k_1=0$. This will only affect a small region centered at the origin of the phase plane, as is corroborated by Fig. 2.

In the absence of the hysteretic friction term, the stability of the origin is predicted by a simple argument given by Landau and Lifshitz [8]. When $k_1\neq0$ the numerical simulations show that the island of arrested motion grows slowly as one moves farther away from parametric resonance ($\omega=2\omega_0$) towards lower frequencies. However, the actual length of the chaotic transients is almost entirely determined by the distribution of the measure on the chaotic attractor. As will be shown below, this distribution is uneven; the more so as the exci-

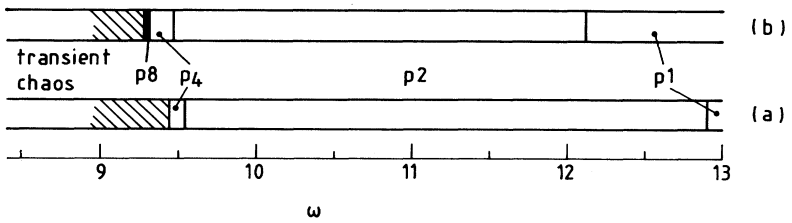

FIG. 3. A part of the phase diagram as a function of the driving frequency ω. Upper, as determined from a numerical simulation; lower, from the experiment. The left bound of the interval of transient chaos is drawn at an arbitrary but short transient length.

tation frequency is increased and the pendulum spends a large fraction of its time away from the origin [13].

Both experiment and simulation exhibit a clear fractal measure in Fig. 4, where in each case 42 754 points are drawn. The measure has a folded leaflike structure and is strongly concentrated near the turnbacks. We will demonstrate that these more concentrated regions of the measure have a scaling behavior that is different from that of the more rarified regions. Therefore, the measures shown in Fig. 4 are multifractal. We will now seek to quantify the observed chaos both through the scaling behavior of the measure and through the unstable periodic cycles.

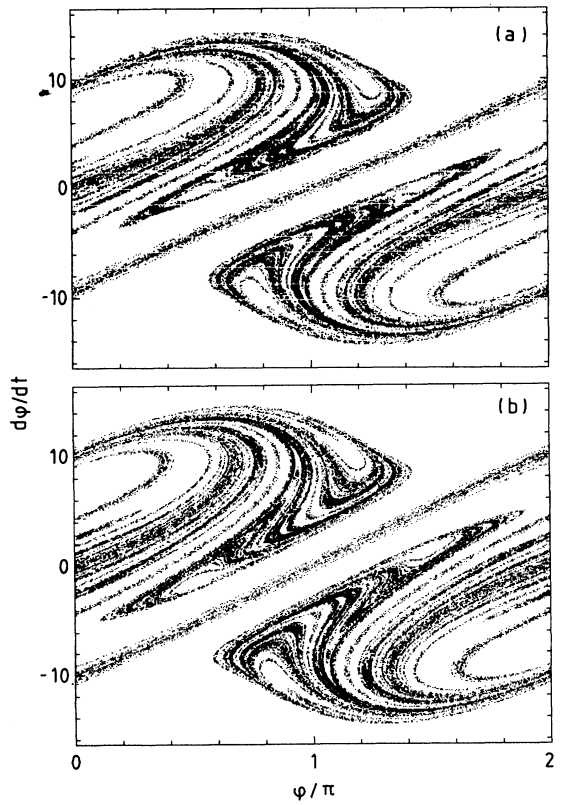

FIG. 4. Poincaré sections of transient chaos during 42 754 cycles: (a) experiment, (b) numerical simulation.

III. MEASURING SCALING BEHAVIOR

The measurement of scaling properties is, in principle, aimed at quantifying the self-similar structure of the attractor. Assume a coverage of the attractor using N balls with sizes $l_i < l$, each of which receives a fraction p_i of the phase-plane points. The scaling of the attractor then follows from considering the partition sum

$$\Gamma(q,\tau)=\sum_{i=1}^{N} p_i^q \Big/ l_i^\tau \ . \tag{3}$$

In the limit of increasingly fine partitions $l \to 0$, the condition $\Gamma(q,\tau)=1$ singles out a dimension $D^q=\tau(q)/(q-1)$ [14]. For partitions with a fixed size l,

$$\sum_{i=1}^{N} p_i^q \simeq l^{(q-1)D^q} \ . \tag{4}$$

The significance of the parameter q is that the more concentrated parts of the attractor may have a different scaling behavior than the more rarely visited. The scaling behavior of these most depleted regions is expressed by D^q with q large and negative, whereas that of the most enhanced regions is expressed by D^q for q large and positive. The point $q=0$ is special in that the capacity dimension D^0 reflects the scaling of the *support* of the measure.

A practical way to measure the function D^q is through the distribution of near-neighbor distances [4,15]. Assume a reference point with index i, we then call $\delta_i(k,n)$ its kth near-neighbor distance out of a set of n points. This distance increases as k increases and decreases as n increases, probing the smallest scales in the measured attractor when n equals the total number of measured phase-space points and $k=1$ (nearest neighbors). Roughly, $\delta_i(k,n) \simeq (k/n)^\beta$, where the value of the local scaling exponent β depends on where the reference point i is located. The generalized dimensions then follow from a generalized average over many (m) such reference points:

$$\delta^{(\gamma)}(k,n) \equiv \left[\frac{1}{m} \sum_{i=1}^{m} [\delta_i^\gamma(k,n)]^\gamma \right]^{1/\gamma} \simeq \left[\frac{k}{n} \right]^{1/D(\gamma)} , \tag{5}$$

where the dimension function $D(\gamma)$ implicitly determines the dimensions D^q: $D(\gamma=(1-q)D^q)=D^q$. Near-neighbor distance scaling may be obtained from measuring either the k or n dependence of $\delta^{(\gamma)}(k,n)$. In practical applications of the method, the k-dependent scaling behavior needs to be corrected by a function that reflects the binomial statistics of near-neighbor distances [15]. Another consequence of the binomial statistics is that in the case of the fixed-k method, which we will employ subsequently, the value of q is bounded by $q<k-1$.

The above-sketched method is one where the mass of partition elements remains fixed, whereas their radius varies. A complementary method to extract generalized dimensions is through the measurement of generalized correlation functions $C^q(l)$ [5]

$$C^q(l)\equiv\left[\frac{1}{m}\sum_{i=1}[M_i(l)]^{q-1}\right]^{1/q-1}\simeq l^{D^q}, \tag{6}$$

where $M_i(l)$ is the number of phase-space points in a ball with radius l around reference point i. This method generates a cover with fixed radius partitions that have varying mass.

In practice, the scaling dynamical range that can be observed in an experiment will be bounded from below by noise. Therefore, care needs to be exercised in applying Eqs. (5) and (6). Depending on the inhomogeneity of the attractor scaling (i.e., the variation of D^q with q), noise may affect the fixed- mass and fixed- radius methods in a different way.

Figure 5(a) shows the scaling behavior of the 16th near-neighbor distance $\delta^{(\gamma=0)}(k=16,n)$ as a function of n both for the experimental and the simulated time series. The moment $\gamma=0$ corresponds to $q=1$; its scaling behavior provides the information dimension. The experimental time series contained 42 754 points and distances were averaged over 8192 reference points; the simulation had 1 048 576 points and 32 768 reference points were used to compute averages. In both cases a clear scaling behavior can be recognized whose dynamical range is limited by the number of phase-plane points. While Fig. 5(a) shows that the D^1 derived from the experiment is in excellent agreement with that of the simulation, determining the scaling behavior of other moments becomes progressively more problematic as $|\gamma|$ increases. This is demonstrated in Fig. 5(b), where we show $\delta^{(\gamma=8)}(k=16,n)$, a moment that is probing the most rarified regions of the measure. Also the scaling using the simulated time series, which does not suffer from noise, shows a clear oscillatory residue. We believe that these problems are due to the la-

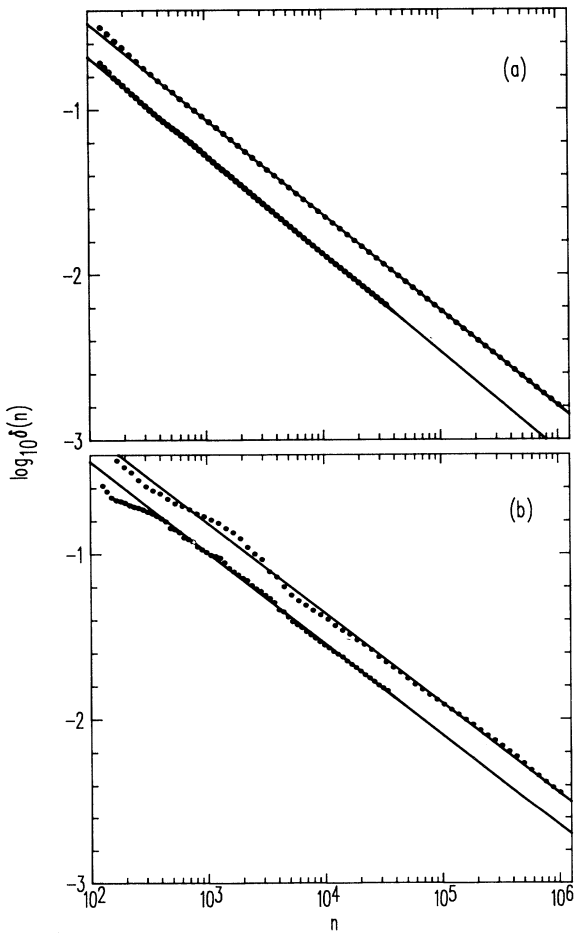

FIG. 5. (a) Dots, scaling functions $\delta^{(\gamma)}(k,n)$ at $k=16$, and $\gamma=0$. Lines, fits using Eq. (5). Upper curve, simulated time series containing 1 048 576 points; lower curve, experimental time series containing 42 754 points. (b) Same as (a) but for $\gamma=8$. For clarity, the simulated results have been shifted vertically in each frame.

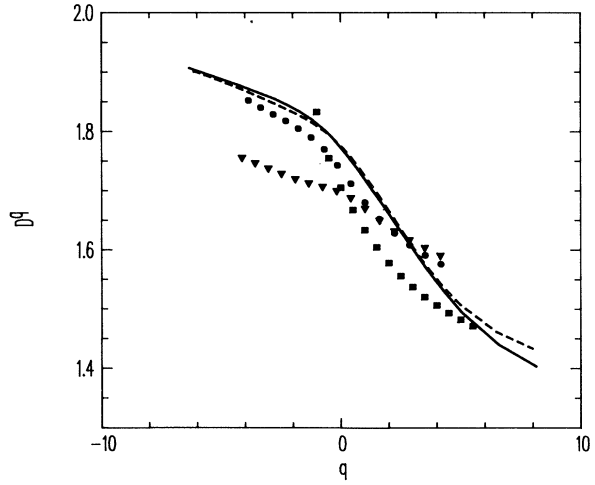

FIG. 6. Spectra of generalized dimensions D^q measured from simulated and experimental time series. Solid line, using near-neighbor distances $\delta^{(\gamma)}(k,n)$ at $k=16$ in the simulated time series. Dashed line, using near-neighbor distances $\delta^{(\gamma)}(k,n)$ at $k=8$ in the simulated time series. Symbols, experiment; balls, using near-neighbor distances $\delta^{(\gamma)}(k,n)$ at $k=16$; triangles, using near-neighbor distances $\delta^{(\gamma)}(k,n)$ at $k=8$; squares, using a variable mass method for the experimental time series.

cunarity of the attractor [16].

The spectra of generalized dimensions, both for the experimental and simulated time series are shown in Fig. 6. In both cases we have used the n dependence of the averaged near-neighbor distance at two values of k ($k=8,16$) and for the experiment we have also employed the fixed-radius method [5]. These various methods give consistent results, leading to the conclusion that the experiment has a multifractal scaling that is in remarkable agreement with that of the simulation.

While the analysis of scaling behavior concentrates on the metric properties of the attractor, it does not provide direct information on the dynamics. It is precisely the dynamics underlying the fractal measure that will be analyzed in the next section, where we will seek the hidden network of low- order periodic orbits.

IV. PERIODIC-ORBIT ANALYSIS

The quest for periodic points and their eigenvalues from a time series begins with partitioning the phase plane into small boxes of linear size ϵ. Next, the points in the time series are sorted with respect to the location of the box to which they belong. This action makes neighboring points in phase space readily accessible: they either belong to the same box or to an adjacent box that can be located swiftly using a binary search. Because most of the time in the algorithm that seeks periodic orbits is spend in finding neighbors, these technicalities dramatically reduce the computing time needed [17].

The length of candidate cycles can then be easily found from the time it takes a single phase-space point to return to within a distance ϵ. Such a point will return to either its own box or to one of the neighboring boxes. Because a point belonging to a p cycle may return each kp step, $k=1,2,\ldots$, it is ascertained that its corresponding entry in the list of return times is p. When multiple cycles return in the same box, this requires a reduction of return times to relative primes. Figure 7 shows a histogram of points in the Pioncaré plane of the experiment that return to within $\epsilon=10^{-2}$ in p steps (ϵ is normalized to unit attractor size). Apparently, the experiment has cycles of length 1 (fixed points) and a number of cycles of even length.

The list of these candidates may be narrowed further by requiring that a box contain at least a few points that ϵ-return as a p cycle. The point $\mathbf{x}_t^p$ that returns closest is selected as a reference point in a local linear approximation A^p of the dynamical system. The stable and unstable eigenvalues of the p-periodic point that are needed, for example, in the cycle expansion of the generalized dimensions, are the eigenvalues of the Jacobian matrix A^p. A least- squares fit was used to estimate the Jacobian matrix A_t^p over a single time step $t,t+1$

$$\mathbf{x}_{t+1}^p-\mathbf{y}_{t+1}=A_t^p(\mathbf{x}_t^p-\mathbf{y}_t)\ . \tag{7}$$

A minimum of 32 neighboring points $\mathbf{y}_t$ was included in the fit; typically, the points were taken from a 2ϵ neighborhood of $\mathbf{x}_t$, excluding those that were within a ϵ_n-noise distance from the reference point (we recall that ϵ_n was estimated to be 5×10^{-3} in the experiment). The cycle Jacobian A^p was then composed out of p single-step Jacobians:

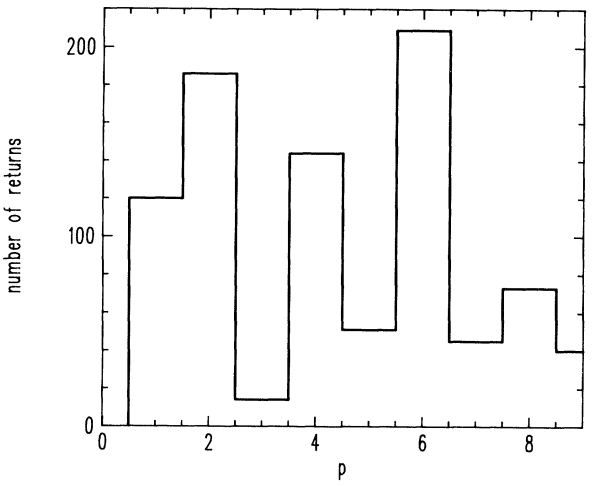

FIG. 7 Number of orbits in the experiment that return in p steps to within $\epsilon=10^{-2}$ as a function of p. The total number of points in the time series is 42 754.

$$A^p=A_{t+p-1}^p A_{t+p-2}^p\cdots A_t^p\ . \tag{8}$$

In principle, identical results should be obtained from a fit of the linear map A^p directly over p time steps; however, the latter poses more severe requirements on the data [18]. The identification of each cycle was facilitated by associating a four-letter symbol with it (the phase plane is divided as $\begin{smallmatrix}A&B\\C&D\end{smallmatrix}$).

The outcome of this procedure is a rather long list of p cycles, each with their stable and unstable eigenvalues. From this list only those p cycles were selected that had entries for each of their p-cycle elements with consistent eigenvalues. Although this attitude may be rather conservative, we will point out below that the marginal hyperbolicity of the chaotic attractor introduces many close returns that are not cycles.

Figure 8(a) shows the cycles up to length 5 that were found in a time series of 42 754 points from the pendulum experiment. The figure nicely illustrates the shadowing mechanism in the central part of the phase plane: long cycles are shadowed by short ones. In almost all cases we did find all p elements of p cycles. If occasionally an element was missed, it was constructed from the companion cycle that is related to it via reflection symmetry of Eq. (2) through the point $((\varphi,\dot{\varphi})=(\pi,0))$ of the phase plane. It is expected that this symmetry also applies to the experiment. The cycles up to length 6 found in a simulated time series of 1 048 576 points are shown in Fig. 8(b). Apparently, the experiment and the simulation have the same network of periodic orbits. The found periodic orbits are concentrated in the region where the attractor is folded strongest and where the measure appears to be concentrated. The fixed point of the upright pendulum

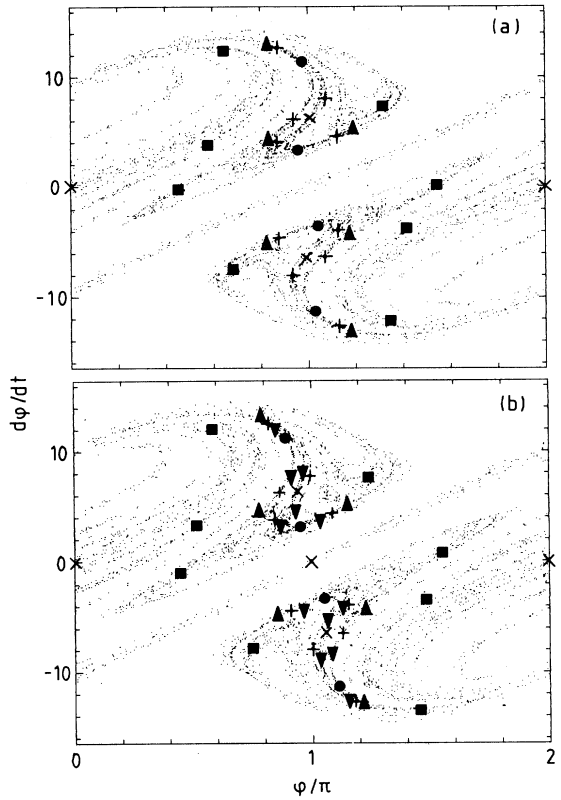

FIG. 8 (a) Experimental attractor overlayed with its low-order periodic points; crosses, circles, triangles, squares, and + signs correspond to periods 1, 2, 3, 4, and 5, respectively. (b) Same as (a), but for the simulated attractor; period-6 orbits are triangles pointing down.

and the period-6 cycle eigenvalue were not found in the experiment, most probably due to the limited number of data points.

Table I summarizes the eigenvalues of the found periodic points together with their symbolic dynamics. It is a striking observation that the shadowing mechanism, predicting cycle eigenvalues that are the product of those of nearby cycles of shorter length is apparently effective for the fixed points, two and six cycles near $\varphi=\pi$ The expanding three- and four-cycle eigenvalues appear in both cases anomalously large. This illustrates the nonuniformity of the measure in the central part of the phase plane. It may very well be, however, that the largest cycle length found here is too small to be able to quantitatively verify shadowing. So far, the shadowing mechanism has only been studied thoroughly in close to 1D attractors [7]. We point out that finding cycles in near-2D systems is much harder.

In Sec. III we compared the scaling properties of the experimental and simulated attractor. The question then quite naturally arises whether these scaling properties can also be predicted by periodic-orbit analysis. In order to connect to the metric properties of the attractor, we must associate the measures p_i and lengths l_i in the partition sum Eq. (3) with the stable and unstable eigenvalues of the periodic points. Regions near such a periodic point are expanded along its unstable direction and contracted along its stable direction. A natural cover, therefore, is one with boxes whose linear size decreases as μ_2, and whose measure decreases as μ_2/μ_1. The generalized dimension D^q then follows from [19]

$$\sum_{\mathrm{fix}(n)} (\mu_1^{(n)})^{-q}(\mu_2^{(n)})^{q-1-\tau}=1 \ , \tag{9}$$

TABLE I. List of cycle eigenvalues that were found from an experimental time series (expt) and those that were determined from a numerical simulation (sim). The phase plane is divided as $\frac{AB}{CD}$, the symbol indicates the order in which the regions A, B, C, and D are visited. For orbits close to the divisor $\varphi=\pi$, the symbol assignment is ambiguous.

Period	No. of cycles	μ_1	μ_2	Symbol	
1	1	2.2	0.37	$\varphi=0$	(expt)
	1	2.01	0.48	$\varphi=0$	(sim)
1	1	36.7	0.028	$\varphi=\pi$	(sim)
1	2	1.68	0.39	*C,B*	(expt)
	2	1.71	0.43	*A,D*	(sim)
2	2	3.8	0.21	*AA, DD*	(expt)
	2	2.54	0.22	*AA, DD*	(sim)
3	2	26	0.067	*ABA,DCD*	(expt)
	2	22.6	0.020	*ABA,DCD*	(sim)
4	2	30	0.02	*ADCB* *ABCD*	(expt)
	2	25.2	0.022	*ADCB* *ABCD*	(sim)
5	2	43	0.008	*AABAB* *CDCDD*	(expt)
	2	43.3	0.0067	*AABAA* *CDDDD*	(sim)
6	2	39.8	0.0015	*ABCBAD* *BCDADC*	(sim)

where the sum over partition elements in Eq. (3) has been replaced by a sum over periodic points. In Eqs. (3) and (9) the value $q=1$ determines the normalization of the measure; the information dimension D^1 merely follows from the continuity requirement. We chose to satisfy the normalization condition by replacing the right-hand side of Eq. (9) with $\sum_{\mathrm{fix}(n)}\mu_2^{(n)}/\mu_1^{(n)}$. As was also emphasized by Cvitanović, Gunaratne, and Procaccia [19], the assumed connection between the metric properties of the attractor and the eigenvalues of its periodic points exclusively applies to measures that are *smooth* along the direction.

We have recast Eq. (9) in terms of a cycle expansion, which means that we approximately allow for cycles that have a length larger than those actually found [20]. First we analyze the numerical simulation whose cycle eigenvalues are listed in Table I. Figure 9 compares the spectrum of generalized dimensions D^q as computed from near-neighbor information with that computed from the eigenvalues of the unstable orbits. It appears that the capacity ($D^{q=0}$) computed from the cycle expansion is in excellent agreement with that computed from the direct method. There is fair agreement for the case $q<0$; however, there is a marked disagreement for the case $q>0$ that corresponds to the more concentrated regions of the phase plane, where the direct method gives a much stronger q dependence of D^q than the cycle expansion. The same conclusions can be reached for the experiment, the results of which are shown in Fig. 10. While there again is a quite remarkable agreement between the dimension spectra near $q=0$, the dimensions corresponding to the more concentrated regions of the phase plane are significantly smaller for the direct method.

It should be realized that the behavior of D^q for $q<0$ is determined by the most depleted regions of phase space

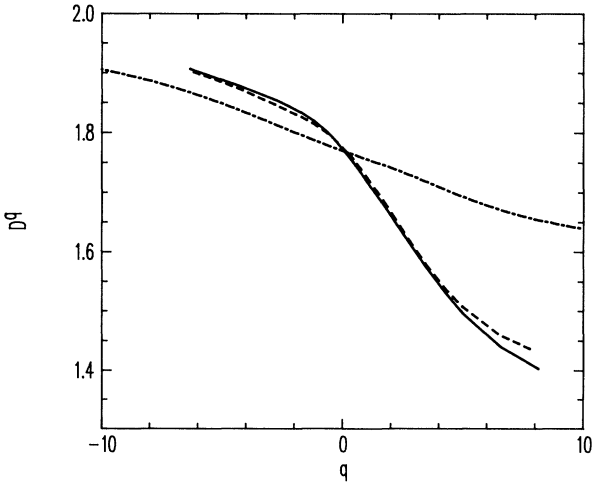

FIG. 9. Generalized dimensions from the numerically simulated time series of 1 048 576 points. Solid and dashed lines, using the direct method of near neighbors at $k=16$ and 8. Dash-dotted line, D^q computed from the unstable orbits listed in Table I.

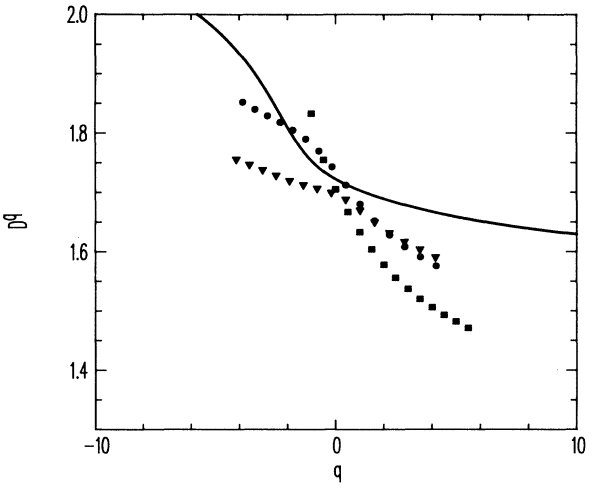

FIG. 10. Generalized dimensions from the experimental time series of 42 754 points. Symbols, generalized dimensions estimated from fixed mass and fixed distance methods (see also Fig. 6). Line, generalized dimensions computed from the experimental unstable periodic orbits listed in Table I.

where we may not be probing the system with sufficient accuracy. Therefore we are not sure of the behavior of D^q for $q<0$. In the case of the cycle expansion it may very well be that the contribution of the most unstable orbits to the cycle expansions is overestimated due to the omission of their shadow companions.

The origin of the differences between direct methods and cycle expansions for $q>0$ is revealed by Fig. 11, which shows an enlargement of the central section of the experimental phase plane. The figure clearly shows the unstable manifolds that emanate from the period-2 cycles. The measure on these manifolds is concentrated at

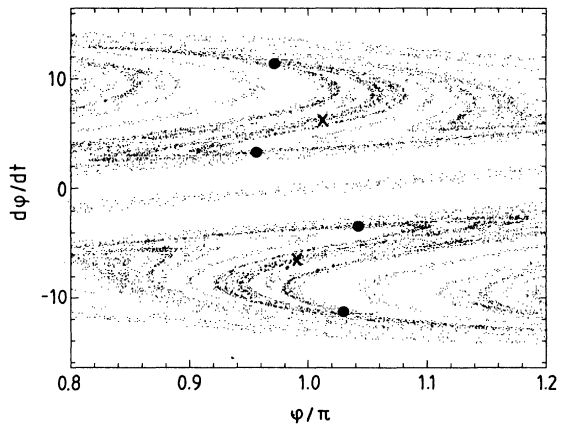

FIG. 11. Enlargement of Fig. 4(a) showing regions of marginal stability. The unstable fixed points are indicated by crosses, the unstable period-2 orbits by circles.

their folding points. These, in fact, are the most concentrated regions of phase space that we probe with $q>0$. Orbits that pass through these folds are marginally stable, the attractor is nonhyperbolic, and the analysis embodied by Eq. (9) is bound to fail. Since folds are mapped on folds and can never be members of a periodic orbit of finite length, nonhyperbolicity will be hard to capture in a cycle description of attractors.

Cvitanović, Gunaratne, and Procaccia [19] have indicated an extension of Eq. (9) that would be applicable in case of marginal hyperbolicity. This method needs orbits of length n in regions of marginal stability, but at the same time necessitates the quest for nearby orbits with the double cycle length $2n$ and *prescribed* symbolic dynamics. In our case, where the attractor is nearly two dimensional and only a small number of cycles can be traced, this is an impossible task.

The presence of such outspoken marginal stability causes close returns near the two-cycle of Fig. 11 that do not correspond to a periodic orbit. These orbits pass close to the folding points and have apparent periods that are even. They are responsible for the peaks in the histogram of close returns (Fig. 7) at multiples of 2. In the simulated time series (where noise is virtually absent) these apparent cycles vanish when the return distance ϵ is made small enough. The experimentalist should be aware of this mechanism that produces close $2p$ returns near a slightly unstable p cycle. When the measure is smooth along the unstable manifold of the p cycle, the apparent $2p$ eigenvalues are the square of the proper p eigenvalues. This was evident in case of the origin fixed point. In fact, this was how the origin eigenvalues in case of the experiment, which has strictly speaking a stable origin, were deduced. The relation between apparent and proper eigenvalues was strongly violated near the nonhyperbolic points shown in Fig. 11.

For lower excitation frequencies, the nonhyperbolicity

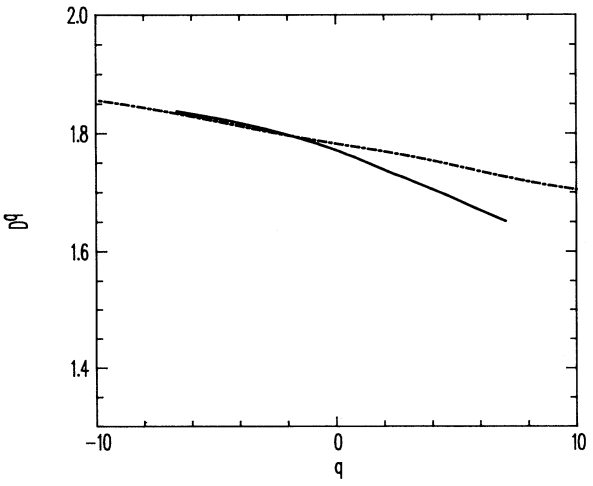

FIG. 12. Generalized dimensions from a numerically simulated time series of 1 048 576 points at $\omega=8.845\ \mathrm{S}^{-1}$. Solid lines using the direct method of near neighbors at $k=16$ and 8. Dash- dotted line, D^q computed from unstable periodic orbits.

diminishes and the chaotic measure is spread out more evenly over the phase plane. Also as a consequence, the spectrum of dimensions becomes flatter. Figure 12 compares the spectra of dimensions D^q computed from near-neighbor scaling and that deduced from a periodic-orbit analysis using a simulated time series at $\omega=8.845\ \mathrm{S}^{-1}$. The dimension spectra are now in perfect agreement for $q<0$, the remaining nonhyperbolicity causing a slight discrepancy at $q\gtrsim 2$. As the pendulum now spends a larger fraction of its time near the origin, the length of the chaotic transient in the experiment has decreased to a few thousand points. Therefore it is not feasible to generate large experimental data sets at this frequency.

When the scaling of the attractor grows more uniform, the terms in a straightforward summation over cycles of the partition function [Eq. (9)] become of a comparable order of magnitude. Therefore, information about *a single cycle* would suffice to estimate D^q. Restricting the summation in Eq. (9) to a single cycle leads, together with the normalization condition, to

$$D^q=1-\frac{\ln\mu_1}{\ln\mu_2}\ , \tag{10}$$

which is the well-known Kaplan-Yorke formula [21]. For the cycles found in the simulation with $\omega=8.845\ \mathrm{S}^{-1}$, Eq. (9) predicts values of D^q in the interval (1.63, 1.95). While this is in fair agreement with the dimensions that were determined using the direct method of near-neighbor scalings, the dimension spectra of the full cycle sum are clearly superior.

V. CONCLUSION

We have demonstrated that it is indeed possible to extract the scaling behavior of a strange attractor from an (experimental) time series of finite length containing finite precision data, through an analysis of its periodic points. Moreover, since a periodic-orbit analysis produces a map of local expansions and contractions, it provides information on strange attractors that is far more valuable than just their average scaling behavior. However, cycle analysis has failed to capture an important qualitative aspect of both experiment and simulation; namely, that they contain marginally stable points. The presence of these points leads to strongly nonuniform scaling behavior.

The exclusive use of time series for finding periodic orbits and their stability raises questions about the data requirements. On the basis of the principle underlying cycle analysis, one is led to believe that it is impossible to derive scaling properties of an attractor if not yet *all* fundamental cycles have been found. However, for our 10^6 simulated points it is already impossible to find orbits of length 8 [22]. Still, we think that direct estimates of scaling properties are possible using data sets that are that large.

Without explicit knowledge of the symbolic dynamics at hand it is impossible to notice that a cycle has been missed. On the other hand, the direct methods to extract scaling behavior may also miss these most depleted regions of phase space, resulting in large errors in D^q for $q<0$. What is clearly needed here is an error analysis of

multifractal scaling measurements.

An important practical problem in our cycle analysis was the large number of close returns that had to be dismissed as cycles. Because we believe that multifractality due to marginal hyperbolicity is quite generic, cycle analysis should be extended to include these close returns that are positioned close to marginally stable points.

ACKNOWLEDGMENTS

The authors thank Dr. James Theiler for generously providing software. They also acknowledge financial support from FOM (Stichting voor Fundamenteel Onderzoek der Materie, the Netherlands).

[1] G. H. Gunaratne, P. S. Linsay, and M. J. Vinson, Phys. Rev. Lett. **63**, 1 (1989).

[2] P. Cvitanović, Phys. Rev. Lett. **61**, 2729 (1988).

[3] H. Poincaré, *Les Méthodes Nouvelles de la Méchanique Céleste* (Gauthier—Villars, Paris, 1892).

[4] K. W. Pettis, T. A. Bailey, A. K. Jain, and R. C. Dubes, IEEE Trans. Pattern Anal. Mach. Intelligence **PAMI-1**, 25 (1979); Y. Termonia and Z. Alexandrowicz, Phys. Rev. **51** 1265 (1983); R. Badii and A. Politi, Phys. Rev. Lett. **52**, 1661 (1984); J. Stat. Phys. **40**, 725 (1985).

[5] K. Pawelzik and H. G. Schuster, Phys. Rev. A **35**, 481 (1987).

[6] A. Chabra and R. V. Jensen, Phys. Rev. Lett. **62**, 1327 (1989).

[7] R. Artuso, E. Aurell, and P. Cvitanović, Nonlinearity **3**, 325 (1990).

[8] L. D. Landau and E. M. Lifshitz, *Mechanics* (Pergamon, New York, 1966).

[9] B. P. Koch, R. W. Leven, B. Pompe, and C. Wilke, Phys. Lett. **96A**, 219 (1983); R. W. Leven, B. Pompe, C. Wilke, and B. P. Koch, Physica **16D**, 371 (1985).

[10] D. P. Lathrop and E. J. Kostelich, Phys. Rev. A **40**, 4028 (1989). Both this article and Ref. [1] concentrate on a characterization of symbolic dynamics via periodic orbits, but do not attempt to estimate metric properties using a cycle analysis. In both cases the attractors studied were close to one dimensional.

[11] The numerical integration of Eq. (2) is slightly complicated by the fact that the angular acceleration suffers a discontinuity when $\dot{\varphi}$ changes sign. This can, however, be adequately handled using a trick described by M. Hénon, Physica Utrecht **5D**, 412 (1982). The values of the parameters used in the simulation were $k_1=6.88\times10^{-4}$, $k_2=4.85\times10^{-4}$, $k_3=1.90\times10^{-4}$, $A=0.131$, $\epsilon=0.173$, $\omega=9.09$, and $\omega_0=5.57$, all in mks units. The largest angular velocity in the freely swinging pendulum that was used to determine the damping constants was 11 rad/s, whereas that in the driven chaotic case is 14 rad/s. This leaves some room for a damping term $O(\dot{\varphi}^3)$ in the driven experiment.

[12] The effect of the hysteretic friction term $k_1\mathrm{sgn}(\dot{\varphi})$ is that the pendulum becomes still at a finite angle φ at some instant t_0. Depending on the phase of the excitation, the pendulum may become unstuck again at a later instant $t, t_0<t<t_0+2\pi/\omega$. This circumstance presents another slight complication in the numerical analysis. The area of the island of arrested motion in the numerical simulation at $\omega=9.09$ is approximately 10^{-5} of that of the phase plane drawn in Fig. 4. The longest chaotic transient that we encountered in the simulation with nonzero hysteretic friction lasted 3×10^4 cycles.

[13] For excitation frequencies that are slightly smaller than $\omega=9.4\ \mathrm{s}^{-1}$ the periodic orbits in the central part of the phase plane are only slightly unstable. This causes strongly intermittent chaos: the pendulum spends a large fraction of its time near these unstable periodic points and only rarely visits the remainder of the phase plane. We have explored other regions of parameter space and believe that this intermittency is the only way to achieve long chaotic transients in the experiment. It may be feasible, however, to redesign the suspension of the pendulum such as to reduce the size of the hysteretic friction term.

[14] R. Benzi, G Paladin, G. Parisi, and A. Vulpiani, J. Phys. A **17**, 3521 (1984); U. Frisch and G. Parisi, in *Turbulence and Predictability in Geophysical Fluid Dynamics and Climate Dynamics* (edited by M. Ghil, R. Benzi, and G Parisi (North-Holland, New York, 1985); T. C. Halsey, M. H. Jensen, L. P. Kadanoff, I. Procaccia, and B. Shraiman, Phys. Rev. A **33**, 1141 (1986).

[15] W. van de Water and P. Schram, Phys. Rev. A **37**, 3118 (1988).

[16] B. B. Mandelbrot, *The Fractal Geometry of Nature* (Freeman, New York, 1983); R. Badii and A. Politi, Phys. Lett. **104A**, 303 (1984); L. A. Smith, J. -D. Fournier, and E. A. Spiegel, *ibid.* **114A**, 465 (1986); W van de Water and P. Schram, *ibid.* **140A** 173 (1989).

[17] This procedure was first described by J. Theiler, Phys. Rev. A **36**, 4456 (1987). Its significance can be appreciated if one realizes that a naive search for neighbors to each of the N data points takes a time proportional to N^2. Rearranging phase space into neighborhoods, on the other hand, takes a time proportional to $N\ln N$, after which the quest for neighbors reduces to either an address lookup or a quick ($\simeq\ln N$) binary search. The program is so fast that a periodic-orbit analysis for up to 28 000 (as limited by a 640-kB memory size) 2D data points can be done in a few minutes of processor time on an ordinary personal computer. The source code is available from the first author.

[18] Over p time steps one would try to deermine A^p from $\mathbf{y}_{t+p-1}-\mathbf{x}^p=A^p(\mathbf{y}_t-\mathbf{x}^p)$. The problem is that the neighborhood of $\mathbf{x}^p$ may spread very rapidly, so that after p time steps it may be very hard to find enough points $\mathbf{y}_{t+p-1}$ that are close enough in time series of manageable length. Furthermore, distances may shrink below the resolution of the experiment in the complementary contracting direction. In the case of very high-quality data it may be feasible to look for the exact return point $\mathbf{x}^p$ by simultaneously fitting A^p and $\mathbf{x}^p$.

[19] P. Cvitanović, G. H. Gunaratne, and I. Procaccia, Phys. Rev. A **38**, 1503 (1988).

[20] The cycle expansion of the generalized dimension uses a dynamical zeta function $\zeta(z)$ that is defined as the following infinite product: $\zeta^{-1}(z)$

$=\prod_p[1-z^{n_p}(u_{1_p})^{-q}(\mu_{2_p})^{q-1-\tau}]$, where p indexes the fundamental cycles (those listed in Table I) with period n_p and stable and unstable eigenvalues μ_{1_p} and μ_{2_p}, respectively. The product is expanded as a polynomial in z, which is truncated with N_p, the highest included order; N_p is the largest cycle length found. The generalized dimension, or equivalently, $\tau(q)$ then follows from the requirement $\zeta^{-1}(z)=0$ for $z=1$. In order to find these zeros it was necessary to omit the fixed point of the pendulum at rest and the very unstable fixed point of the upright pendulum at $(\varphi,\dot{\varphi})=(\pi,0)$ from the expansion and to include them in an ordinary fashion as in Eq. (9).

[21] J. L. Kaplan and J. A. Yorke, in *Functional Differential Equations and Approximation of Fixed Points,* edited by H. O. Peitgen and H. O. Walther, Lecture Notes in Mathematics Vol. 730 (Springer, Berlin, 1979), p. 204.

[22] Assuming a uniform dimension D, the number of points in a time series of length n that are close to a cycle and return within ϵ is $(\mu_2/\mu_1)\epsilon^D n$. If we take typical values of Table I as average expansion and contraction rates per time step, 1.5 and 0.4, respectively, a period-8 cycle would have $\mu_1\cong(1.5)^8$, $\mu_2\cong(0.4)^8$. In that case at least 3×10^6 points would be needed for observation of a single return in $\epsilon=10^{-1}$.